Catalysis Science & Technology

Accepted Manuscript

ROYAL SOCIETY OF CHEMISTRY

www.rsc.org/catalysis

Catalysis Science & Technology

ARTICLE

Self-assembled synthesis of reduced graphene oxide supported platinum nanowires composites with enhanced electrocatalytic activity towards the hydrazine oxidation reaction

Received 00th January 20xx,
Accepted 00th January 20xx

DOI: 10.1039/x0xx00000x

www.rsc.org/

Xueqing Gao‡[a], Yigang Ji‡[b], Shan He [a], Shuni Li [a,]*, Jong-Min Lee [c,]*

The reduced graphene oxide (RGO) supported Pt nanocrystals composites have wide applications in catalysis and electrocatalysis. In this work, we successfully synthesize guanidine-functionalized graphene oxide composites and phosphonate-functionalized platinum nanowires (Pt-NWs). Based on self-assembly and $NaBH_4$ reduction, RGO supported Pt-NWs composites (Pt-NWs/RGO) are obtained successfully. The as-prepared nanomaterials are detailedly characterized by various physical techniques, such as transmission electron microscopy, X-ray photoelectron spectroscopy, X-ray diffraction, and element mapping, *etc*. Physical characterization results demonstate that the guanidine functionalization of graphene oxide is crucial for the generation of Pt-NWs/RGO composites. Electrochemical results show both the phosphonate functionalization of Pt-NWs and the introduction of RGO contribute to the improved electrocatalytic activity of Pt-NWs/RGO composites towards the hydrazine oxidation reaction.

Introduction

The carbon materials supported Pt-based nanocrystal composites are highly efficient anode and cathode elecrocatlysts in various low-temperature polymer electrolyte fuel cells, such as direct methanol fuel cells, direct formic acid fuel cells, and direct hydrazine fuel cells, *etc*.[1-16] It is well known that the utilization, activity, and durability of Pt/carbon composites highly depend on the nature of carbon materials and morphology of Pt nanocrystals. Compared with zero-dimensional Pt nanoparticles, one-dimensional Pt nanowires (Pt-NWs) effectively decrease the Ostwald ripening effect, improve electron transport, and accelerate mass transport of reactants due to their inherent anisotropic morphology and unique structure,[17-22] which impart Pt-NWs with much improved electrocatalytic activity and durability for many important electrochemical reactions, such as oxygen reduction reaction,[17-19] methanol oxidation reaction,[20] hydrogen evolution reaction,[21] and formic acid oxidation reaction,[22] *etc*.

Two-dimensional graphene, a star carbon material, has extraordinary electronic transport property, big surface area, and high chemical stability, which make it one of the most ideal support materials.[23-32] For graphene supported zero-dimensional noble metal nanoparticles composites, however, the serious re-stacking of graphene nanosheets may limit the access of electrolytes to the internal surface of graphene, which reduces the overall utilization of noble metal.[33-37]

Recently, the assembly of one-dimensional Pt-NWs into two-dimensional graphene has attracted remarkable attention. Like carbon nanotubes/graphene composites,[38-40] the graphene/Pt-NWs composites improve the accessibility of the electrolyte due to the particularly the three-dimensional structure of composites, and show enhanced eletrocatalytic activity and durability for electrochemical oxidation or reduction of fuel molecules due to the high electrical conductivity of graphene and and efficient anchorage of nanoparticles on graphene that effectively restrains the aggregation and Ostwald ripening.[33, 41, 42]

Hydrazine is widely used as the raw materials in the chemical industry and pharmaceutical field, including rocket fuels, water treatment, plant growth regulators, and direct hydrazine fuel cells. The electrocatalytic oxidation of hydrazine has attracted the substantial interest for the development of direct hydrazine fuel cells and electrochemical sensing.[43-50] Due to excellent electrocatalytic activity of Pt nanocrystals towards the hydrazine oxidation reaction (HOR), the HOR on various Pt nanocrystals with different morphology and Pt/support materials composites, such as pine-shaped Pt nanostructures,[51] Pt nanoclusters,[52] Au@Pt core–shell nanoparticles,[53] Pt/TiO_2 hybrid nanofibers,[54] Pt nanoparticles/nitrogen-graphene,[55] and Pt nanoparticles/mesoporous carbon,[56] has been investigated widely. To the best of our knowledge, however, there has been no report on the HOR on Pt-NWs as well as graphene/Pt-NWs composites. In this work, we successfully synthesized guanidine-functionalized graphene oxide composites ($GO@NH_2$) and phosphonate-functionalized Pt-NWs (Pt-NWs-P).

[a] *Key Laboratory of Macromolecular Science of Shaanxi Province, School of Chemistry & Chemical Engineering, Shaanxi Normal University, Xi'an 710062, PR China E–mail: lishuni@snnu.edu.cn (S. Li)*
[b] *Department of Life Sciences and Chemistry, Jiangsu Second Normal University, Nanjing 210013, PR China*
[c] *School of Chemical and Biomedical Engineering, Nanyang Technological University, Singapore 637459, Singapore E–mail: jmlee@ntu.edu.sg (J.-M. Lee)*
‡ These two authors made an equal contribution to this work.

Then, the reduced graphene oxide (RGO) supported Pt-NWs composites (Pt-NWs/RGO) were obtained by the self-assembly of Pt-NWs-P on GO@NH_2, accompanied with a followed $NaBH_4$ chemical reduction. The as-prepared Pt-NWs/RGO composites exhibited improved electrocatalytic activity towards the HOR compared to un-supported Pt-NWs and commercial Pt/C electrocatalyst.

Experimental

Reagents and chemicals

Graphene oxide (GO) was purchased from Nanjing XFNANO Materials TECH Co., Ltd. Guanidine hydrochloride (Scheme 1) was supplied from ChengJie Chem. Co., Ltd. Ethylenediamine-tetramethylene phosphonic acid (EDTMP, Scheme 1) was purchased from Shandong Taihe Water Treatment Co., Ltd. The commercial 40 wt.% Pt/C electrocatalyst was obtained from E-TEK Division, PEMEAS Fuel Cell Technologies. Other chemicals were of analytical reagent grade and used without further purification.

Synthesis of Pt-NWs/RGO composites

The schematic synthesis procedure of Pt-NWs/RGO composites was shown in Scheme 1.

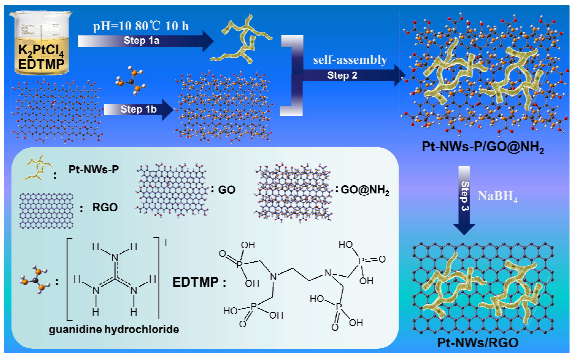

Scheme 1. Schematic synthetic route of Pt-NWs/RGO composites.

Step 1a: The synthesis of phosphonate-functionalized Pt-NWs (Pt-NWs-P). According to the improved self-reduction method,[57] Pt-NWs-P were obtained by heating 15 mL of mixture solution containing 2.5 mM K_2PtCl_4 and 3 mM EDTMP mixture solution (pH 10) for 10 h at 80°C. After collecting by centrifugation, the obtained Pt-NWs-P composites were re-dispersed in 10 mL water by sonication.

Step 1b: The synthesis of guanidine-functionalized GO (GO@NH_2). Based on the π–π stacking interaction between GO and guanidine, GO@NH_2 was easily synthesized by sonicating 10 mL of mixture solution containing 0.1706 g guanidine hydrochloride (Scheme 1) and 5.0 mg GO for 60 min at room temperature. After collecting by centrifugation and washing, the as-prepared GO@NH_2 composites were re-dispersed in 10 mL water by sonication.

Step 2. The self-assembly of Pt-NWs-P on GO@NH_2. In a typical procedure, 10 mL of 0.348 mg mL^{-1} Pt-NWs-P suspension and 10 mL of 0.5 mg mL^{-1} GO@NH_2 were mixed and sonicated for 2 h.

Step 3. The reduction of GO to RGO. In a typical synthesis, 10 mL of 0.5 M $NaBH_4$ solution was added into the above Pt-NWs-P/GO@NH_2 suspension and stirred for 60 min. After reaction, the obtained Pt-NWs/RGO composites were separated by centrifugation, and then dried in a vacuum dryer.

Electrochemical measurements

CHI 660 D electrochemical analyzer was used to perform all electrochemical measurements at 30 ± 1 °C. Saturated calomel electrode served as the reference electrode, catalyst modified glassy carbon electrode acted as the work electrode, Pt wire was used as the counter electrode. Electrode potentials in this work were given versus the reversible hydrogen electrode (RHE). The Nafion covered catalyst modified electrode was prepared according to the procedure reported previously.[58] The loading of the catalyst on the glassy carbon electrode was ca. 216.7 μg cm^{-2}. The electrochemical impedance spectroscopy (EIS) measurements were performed at open circuit potential from 0.1～100,000 Hz with a modulation amplitude of 5 mV. In order to avoid the interference of the produced N_2 bubbles, chronoamperometry tests were conducted on the Gamry's Rotating Disk Electrode (RDE710) at 2000 rpm rotation.

Instruments

The ultraviolet and visible spectroscopy (UV−vis, Shimadzu UV2600) was used to investigate the interaction between guanidine hydrochloride and GO. Transmission electron microscopy (TEM, JEM-2100F) was used to characterize the morphology and size of samples. X-ray photoelectron spectroscopy (XPS, AXIS ULTRA) and zeta potential analyzer (Malvern Zetasizer Nano ZS90) were used to analyze the surface composition and charge of samples. The Pt loading on Pt-NWs/RGO composites was determined by inductively coupled plasma atomic emission spectrum (ICP-AES). The element distribution of the sample was investigated by energy-dispersive X-ray (EDX) mapping analysis (JSM-2010). X-ray diffraction (XRD, D/max-rC) was used to study the crystal structure of samples.

Results and discussion

Characterization of Pt-NWs-P

Compared to previous synthesis at 60°C by Prof. Chen,[57] in the present work, the synthesis time of Pt-NWs-P was reduced from 48 h to 10 h after elevating the reaction temperature to 80°C. TEM images reveal the diameter of the Pt-NWs-P is ca. 3.5 nm, and the Pt-NWs-P have abundant Pt(111) facets (Fig. 1AB). XPS measurements clearly display the N1s and P2p signals (Fig. 1C). The zeta potential of the Pt-NWs-P is −40 mV at pH 7.0, in consistent with the previous report,[57] confirming the phosphonate functionalization of Pt-NWs. Herein, the aminophosphonate molecules (*i.e.*, the oxidation products of EDTMP) adsorb on Pt-NWs surface via N-Pt bond whereas the negatively charged phosphonate groups are exposed to the outside of Pt-NWs.[57, 59, 60] EDX element mapping patterns show that both N and P element patterns are similar to Pt element pattern, which demonstrates the uniform distribution of aminophosphonate on Pt-NWs surface (Fig. 1D).

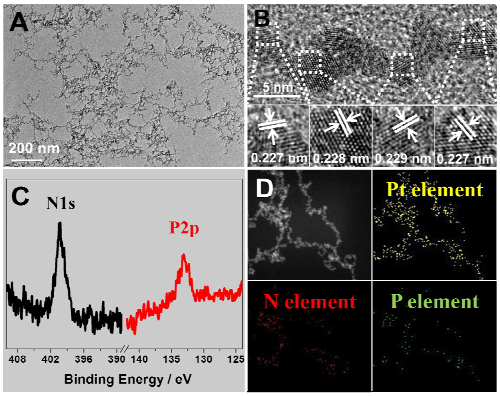

Fig. 1 (A) TEM and (B) HRTEM images of Pt-NWs-P. (C) N1s and P2p XPS spectra of Pt-NWs-P. (D) Representative high-angle annular dark-field scanning TEM image of Pt-NWs-P and corresponding EDX element mapping.

Characterization of GO@NH_2

The π–π stacking and electrostatic attractions are the two primary driving forces for the noncovalent functionalization of GO. Since the positively charged guanidine ion is a planar π-conjugated molecule, the guanidine ion may easily adsorb on the GO surface. The interactions between guanidine hydrochloride and GO were investigated by UV-Vis. As observed, guanidine hydrochloride shows a small hump peak at ca. 260.6 nm and 280.3 nm (Fig. 2A-a). Compared to the maximum absorption peak of GO at 228.3 nm (Fig. 2A-b), the maximum absorption peak of GO@NH_2 shifts negatively to 215.9 nm (Fig. 2A-c). The redshift demonstrates the chemical functionalization of GO by guanidine.[61] The generation of GO@NH_2 was chemically confirmed by XPS. The appearance of the N1s peak at 397.6 eV confirms the adsorption of guanidine on the GO surface (Fig. 2B). The zeta potential of GO is –45.6 mV whereas the zeta potential of GO@NH_2 is −24.3 mV. The change in the surface charge also confirms the adsorption of the guanidine ion on the GO surface. The distribution of guanidine on the GO surface was visualized by EDX element mapping. The similarity between N element pattern and C element pattern demonstrates the uniform distribution of guanidine ion on the GO surface (Fig. 2C).

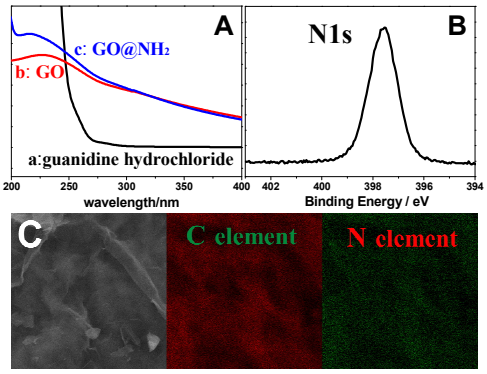

Fig. 2 (A) UV-vis spectra of (a) guanidine hydrochloride, (b) GO and (c) GO@NH_2. (B) N1s XPS spectrum of GO@NH_2. (C) Representative SEM image of GO@NH_2 and corresponding EDX element mapping.

Self-assembly of Pt-NWs-P on GO@NH_2

The chemical functionalization of GO is crucial for the anchorage of Pt-NWs-P on the GO surface. As observed, the gray-black Pt-NWs-P still suspends in the mixture after sonicating the mixture of Pt-NWs-P and GO (Fig. 3A), indicating that Pt-NWs-P can't completely adsorb on GO due to electrostatic repulsion between the negatively charged Pt-NWs-P and the negatively charged GO. In sharp contrast, the complete precipitate is obtained after sonicating the mixture of Pt-NWs-P and GO@NH_2 (Fig. 3B), indicating the efficient anchorage of Pt-NWs-P on GO@NH_2 due to the electrostatic attraction. This discrepancy was confirmed by TEM. Few Pt-NWs-P are observed at the GO surface (Fig. 3C) whereas a large number of Pt-NWs-P are found at the GO@NH_2 surface (Fig. 3D), confirming the guanidine functionalization of GO favors the anchorage of Pt-NWs-P due to the electrostatic attraction.

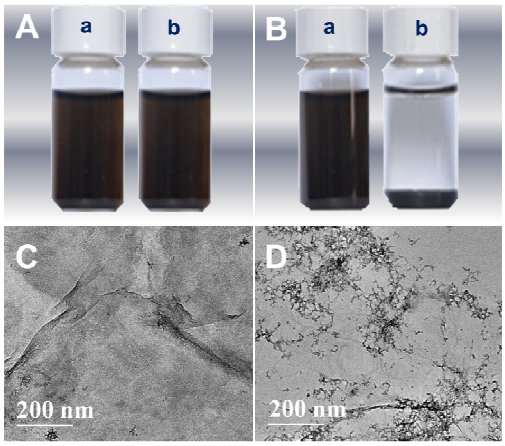

Fig. 3 (A) Photographs of the mixture solution containing Pt-NWs-P and GO (a) before and (b) after sonicating for 1 h. (B) Photographs of the mixture solution containing Pt-NWs-P and GO@NH_2 (a) before and (b) after sonicating for 1 h. Representative TEM images of (C) Pt-NWs-P/GO and (D) Pt-NWs-P/GO@NH_2 composites.

Characterization of Pt-NWs/RGO composites

The Pt loading and crystal structure of Pt-NWs/RGO composites were characterized by ICP-AES and XRD. The actual Pt contents in Pt-NWs/RGO composites is measured to be 37.0 wt. %. The XRD pattern of Pt-NWs/RGO composites shows the four characteristic diffraction peaks of (111), (200), (220) and (311) facets (Fig. 4A), matching with the standard value of the face centred cubic Pt crystal well (JCPDS no. 04-0802 Pt). Meanwhile, the strong C(002) diffraction peak of GO at ca. 12.5° disappears and a weak C(002) diffraction peak of RGO is found in the XRD pattern of Pt-NWs/RGO, indicating the GO is reduced to RGO by $NaBH_4$. Compared to C1s XPS spectrum of GO, the peak intensities of C–OH, HO–C=O and C–O–C at Pt-NWs/RGO composites decrease remarkably (Fig. 4B), further confirming the reduction of GO. The generation of RGO is expected to significantly enhance the electrical conductivity of composites, which facilitates the electron transfer in various electrochemical reactions.[26] Further TEM measurements show the morphology and crystal facets of Pt-NWs-P on Pt-NWs/RGO composites still retain well after the reduction of GO by $NaBH_4$ (Fig. 4C), indicating the assembly-reduction strategy is an efficient method for the synthesis of high-quality metal/RGO composites.

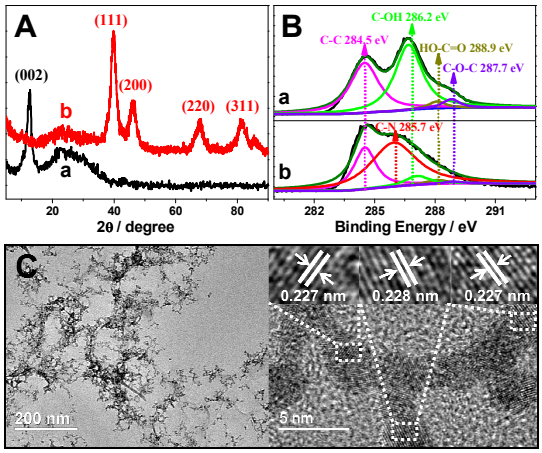

Fig. 4 (A) XRD patterns of (a) GO and (b) Pt-NWs/RGO composites. (B) C1s XPS spectra of (a) GO and (b) Pt-NWs/RGO composites. (C) TEM images of Pt-NWs/RGO composites.

Electrocatalytic activity of Pt-NWs/RGO composites

The electrochemical property of Pt-NWs/RGO composites is first investigated by cyclic voltammetry (CV) in the 0.1 M N_2-saturated H_2SO_4 solution (Fig. 5A). For comparison, the electrochemical properties of Pt-NWs-P and commercial Pt/C electrocatalyst were also investigated. The electrochemically active surface area (ECSA) of electrocatalysts is calculated by integrating hydrogen adsorption charges.[19] The ECSA (35.5 m^2 g^{-1}) of Pt-NWs-P is close to that (42.1 m^2 g^{-1}) of the commercial Pt/C electrocatalyst but lower than that (60.5 m^2 g^{-1}) of Pt-NWs/RGO composites. The anchorage of Pt-NWs-P on RGO effectively restrains the re-aggregation of Pt-NWs-P during the preparation of the modified electrode, which contributes to the increased ECSA of Pt-NWs/RGO composites compared to Pt-NWs-P.

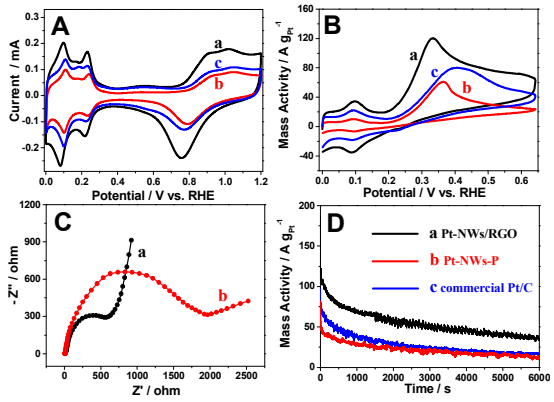

Fig. 5 (A) CV curves of (a) Pt-NWs/RGO composites, (b) Pt-NWs-P and (c) commercial Pt/C electrocatalyst in N_2-saturated 0.1 M H_2SO_4 solution at a scan rate of 50 mV s^{-1}. (B) The Pt mass-normalized CV curves of (a) Pt-NWs/RGO composites, (b) Pt-NWs-P and (c) commercial Pt/C electrocatalyst in N_2-saturated 0.1 M H_2SO_4 + 0.01 M N_2H_4 solution at a scan rate of 50 mV s^{-1}. (C) EIS curves of (a) Pt-NWs/RGO composites and (b) Pt-NWs-P in N_2-saturated 0.1 M H_2SO_4 + 0.01 M N_2H_4 solution at open circuit potential. (D) Chronoamperometry curves of (a) Pt-NWs/RGO composites, (b) Pt-NWs-P and (c) commercial Pt/C electrocatalyst in N_2-saturated 0.1 M H_2SO_4 + 0.01 M N_2H_4 solution for 6000 at 0.30 V at 2000 rpm rotation rate.

The electrocatalytic activities of electrocatalysts towards the hydrazine oxidation reaction (HOR) were examined by CV, using the same Pt loading. Compared to Pt-NWs-P, Pt-NWs/RGO composites show the lower onset oxidation potential and higher oxidation peak current (Fig. 5B), demonstrating the remarkably enhanced electrocatalytic activity. EIS measurements show the charge transfer impedance of Pt-NWs/RGO composites (R_{ct}=710.7Ω) is smaller than that of Pt-NWs (R_{ct}=1742 Ω) towards the HOR (Fig. 5C), indiating the introduction of RGO facilitates the electron transfer of the HOR. Thus, the improved electrocatalytic mass activity can be ascribed to the bigger ECSA of Pt-NWs/RGO composites and lower electron transfer resistance compared to Pt-NWs-P. The electrocatalytic activity and stability of electrocatalysts towards the HOR were further investigated by chronoamperometry. In the whole process, the HOR current on Pt-NWs/RGO composites is higher than that on Pt-NWs-P (Fig. 5D), confirming their high activity and durability. Specially, both Pt-NWs/RGO composites and Pt-NWs-P show the lower oxidation peak potential towards the HOR compared to the commercial Pt/C electrocatalyst (Fig. 5B), indicating the phosphonate functionalization of Pt-NWs accelerates the reaction kinetics of the HOR. Likely, the electrostatic attraction between the positively charged $N_2H_5^+$ ion and the negatively charged phosphonate groups results in enrichment of hydrazine on the Pt surface, which improves the eletrocatalytic activity of Pt towards the HOR, similar to the case of the electrooxidation of dopamine on a phosphonate functionalized Au electrode.[62] Moreover, both CV and chronoamperometry measurements show the electrocatalytic activity and stability of Pt-NWs/RGO composites are much better than the commercial Pt/C electrocatalyst, which is done by evaluating peak current and pseudo steady state current of the HOR at electrocatalysts (Fig. 5B and D). The present experimental results suggest that Pt-NWs/RGO composites hold promise as potentially practical electrocatalyst towards the HOR.

Conclusions

We develop a self-assembly/chemical-reduction two-step route to efficiently synthesize Pt-NWs/RGO composites with high shape selectivity based on electrostatic attraction between Pt-NWs-P and GO@NH_2. The introduction of RGO enhances the electrocatalytic activity of Pt-NWs-P towards the HOR due to the improved dispersion of Pt-NWs-P and the reduced electron transfer resistance. Phosphonate functionalization of Pt-NWs accelerates the reaction kinetics of the HOR due to the electrostatic interaction between the $N_2H_5^+$ ions and phosphonate groups. The electrocatalytic activity and stability of Pt-NWs/RGO composites are much better than the commercial Pt/C electrocatalyst, suggesting Pt-NWs/RGO composites have potentially practical application towards the HOR.

Acknowledgements

This work was supported by National Natural Science Foundation of China (21301114), Natural Science Foundation of Shaanxi Province (2013JQ2009), Foundation of the Jiangsu Education Committee (14KJD150002), Jiangsu Key Laboratory

of Biofuction Molecule, and the Academic Research Fund of the Ministry of Education in Singapore (RGT27/13).

Notes and references

1. Y. Nie, S. Chen, W. Ding, X. Xie, Y. Zhang and Z. Wei, *Chem. Commun.*, 2014, **50**, 15431-15434.
2. A. Saito, H. Tsuji, I. Shimoyama, K. i. Shimizu and Y. Nishina, *Chem. Commun.*, 2015, **51**, 5883-5886.
3. C. Zhang, L. Xu, N. Shan, T. Sun, J. Chen and Y. Yan, *ACS Catal.*, 2014, **4**, 1926-1930.
4. J. Zhao, L. Zhang, T. Chen, H. Yu, L. Zhang, H. Xue and H. Hu, *J. Phys. Chem. C*, 2012, **116**, 21374-21381.
5. K. Okaya, H. Yano, K. Kakinuma, M. Watanabe and H. Uchida, *ACS Appl. Mater. Inter.*, 2012, **4**, 6982-6991.
6. C. Yang, M. Zhou and Q. Xu, *Nanoscale*, 2014, **6**, 11863-11870.
7. Y. Lim, S. K. Kim, S. C. Lee, J. Choi, K. S. Nahm, S. J. Yoo and P. Kim, *Nanoscale*, 2014, **6**, 4038-4042.
8. S. C. Sahu, A. K. Samantara, B. Satpati, S. Bhattacharjee and B. K. Jena, *Nanoscale*, 2013, **5**, 11265-11274.
9. L. Chen, Y. Bao, Y. Sun, D. Ma, D. Ye and B. Huang, *Catal. Sci. Technol.*, 2015, DOI: 10.1039/c5cy01091h.
10. İ. Esirden, E. Erken, M. Kaya and F. Sen, *Catal. Sci. Technol.*, 2015, **5**, 4452-4457.
11. A. V. Kirilin, B. Hasse, A. V. Tokarev, L. M. Kustov, G. N. Baeva, G. O. Bragina, A. Y. Stakheev, A. R. Rautio, T. Salmi, B. J. M. Etzold, J. P. Mikkola and D. Y. Murzin, *Catal. Sci. Technol.*, 2014, **4**, 387-401.
12. S. Jafar Hoseini, M. Dehghani and H. Nasrabadi, *Catal Sci Technol*, 2014, **4**, 1078-1083.
13. S. Li, H. Yang, Z. Dong, S. Guo, J. Zhao, G. Gou, R. Ren, J. Huang, J. Jin and J. Ma, *Catal. Sci. Technol.*, 2013, **3**, 2303-2310.
14. B. Habibi and N. Delnavaz, *RSC Advances*, 2015, **5**, 73639-73650.
15. W. Liu, C. Li, P. Zhang, L. Tang, Y. Gu, Y. Zhang, J. Zhang, Z. Liu, G. Sun and Z. Zhang, *RSC Adv.*, 2015, **5**, 73993-74002.
16. S. R. Suryawanshi, V. Kaware, D. Chakravarty, P. S. Walke, M. A. More, K. Joshi, C. S. Rout and D. J. Late, *RSC Adv.*, 2015, **5**, 80990-80997.
17. C. Koenigsmann, W.-p. Zhou, R. R. Adzic, E. Sutter and S. S. Wong, *Nano Lett.*, 2010, **10**, 2806-2811.
18. S. J. Percival and B. Zhang, *J. Phys. Chem. C*, 2013, **117**, 13928-13935.
19. S. H. Sun, G. X. Zhang, D. S. Geng, Y. G. Chen, R. Y. Li, M. Cai and X. L. Sun, *Angew. Chem. Int. Edit.*, 2011, **50**, 422-426.
20. L. Zhang, N. Li, F. Gao, L. Hou and Z. Xu, *J. Am. Chem. Soc.*, 2012, **134**, 11326-11329.
21. H. Yin, S. Zhao, K. Zhao, A. Muqsit, H. Tang, L. Chang, H. Zhao, Y. Gao and Z. Tang, *Nat. commun.*, 2015, **6**, 6430.
22. B. Y. Xia, H. B. Wu, Y. Yan, X. W. Lou and X. Wang, *J. Am. Chem. Soc.*, 2013, **135**, 9480-9485.
23. H. Feng, Y. Liu and J. Li, *Chem. Commun.*, 2015, **51**, 2418-2420.
24. Z. Xia, S. Wang, L. Jiang, H. Sun, F. Qi, J. Jin and G. Sun, *J. Mater. Chem. A*, 2015, **3**, 1641-1648.
25. L. Zhao, Z. B. Wang, J. L. Li, J. J. Zhang, X. L. Sui and L. M. Zhang, *J. Mater. Chem. A*, 2015, **3**, 5313-5320.
26. G. R. Xu, J. J. Hui, T. Huang, Y. Chen and J. M. Lee, *J. Power Sources*, 2015, **285**, 393-399.
27. M. Zhang, Z. Yan, Y. Li, J. Jing and J. Xie, *Electrochimica Acta*, 2015, **161**, 48-54.
28. M. Sekkarapatti Ramasamy, A. Nikolakapoulou, D. Raptis, V. Dracopoulos, G. Paterakis and P. Lianos, *Electrochim. Acta*, 2015, **173**, 276-281.
29. G. Chang, H. Shu, Q. Huang, M. Oyama, K. Ji, X. Liu and Y. He, *Electrochim. Acta*, 2015, **157**, 149-157.
30. L. Yang, Y. Tang, S. Luo, C. Liu, H. Song and D. Yan, *ChemSusChem*, 2014, **7**, 2907-2913.
31. C. Liu, H. Zhang, Y. Tang and S. Luo, *Journal of Materials Chemistry A*, 2014, **2**, 4580-4587.
32. L. Yang, D. Yan, C. Liu, H. Song, Y. Tang, S. Luo and M. Liu, *J. Power Sources*, 2015, **278**, 725-732.
33. S. Du, Y. Lu and R. Steinberger Wilckens, *Carbon*, 2014, **79**, 346-353.
34. X. Dong, X. Wang, L. Wang, H. Song, H. Zhang, W. Huang and P. Chen, *ACS Appl. Mater. Inter.*, 2012, **4**, 3129-3133.
35. C. Li and G. Shi, *Nanoscale*, 2012, **4**, 5549-5563.
36. A. Marinkas, F. Arena, J. Mitzel, G. M. Prinz, A. Heinzel, V. Peinecke and H. Natter, *Carbon*, 2013, **58**, 139-150.
37. E. Antolini, *Appl. Catal. B-Environ.*, 2012, **123**, 52-68.
38. Y. Li, W. Zhou, H. Wang, L. Xie, Y. Liang, F. Wei, J.-C. Idrobo, S. J. Pennycook and H. Dai, *Nat. nanotechnol.*, 2012, **7**, 394-400.
39. S. Nardecchia, D. Carriazo, M. L. Ferrer, M. C. Gutierrez and F. del Monte, *Chem. Soc. Rev.*, 2013, **42**, 794-830.
40. S. H. Lee, D. H. Lee, W. J. Lee and S. O. Kim, *Adv. Funct. Mater.*, 2011, **21**, 1338-1354.
41. M. A. Hoque, F. M. Hassan, D. Higgins, J. Y. Choi, M. Pritzker, S. Knights, S. Ye and Z. Chen, *Adv. Mater.*, 2014, **7**, 1229-1234.
42. Z. Luo, L. Yuwen, B. Bao, J. Tian, X. Zhu, L. Weng and L. Wang, *J. Mater. Chem.*, 2012, **22**, 7791-7796.
43. F. Zhang, L. Zhang, J. Xing, Y. Tang, Y. Chen, Y. Zhou, T. Lu and X. Xia, *ChemPlusChem*, 2012, **77**, 914-922.
44. J. Zhao, M. Zhu, M. Zheng, Y. Tang, Y. Chen and T. Lu, *Electrochim. Acta*, 2011, **56**, 4930-4936.
45. J. Li and X. Q. Lin, *Sensor. Actuat. B-Chem.*, 2007, **126**, 527-535.
46. S. Virji, R. B. Kaner and B. H. Weiller, *Chem. Mater.*, 2005, **17**, 1256-1260.
47. B. K. Jena and C. R. Raj, *J. Phys. Chem. C*, 2007, **111**, 6228-6232.
48. K. Asazawa, K. Yamada, H. Tanaka, A. Oka, M. Taniguchi and T. Kobayashi, *Angew. Chem. Int. Edit.*, 2007, **46**, 8024-8027.
49. Y. Ma, H. Li, R. Wang, H. Wang, W. Lv and S. Ji, *J. Power Sources*, 2015, **289**, 22-25.
50. L. Tamašauskaitė Tamašiūnaitė, J. Rakauskas, A. Balčiūnaitė, A. Zabielaitė, J. Vaičiūnienė, A. Selskis, R. Juškėnas, V. Pakštas and E. Norkus, *J. Power Sources*, 2014, **272**, 362-370.
51. A. Ponrouch, S. Garbarino, E. Bertin, C. Andrei, G. A. Botton and D. Guay, *Adv. Funct. Mater.*, 2012, **22**, 4172-4181.
52. Y. Zhou, L. Tang, X. Xie, G. Zeng, J. Gong, D. Huang, Y. Zhang, G. Yang, J. Wang and C. Zhang, *Curr. Anal. Chem.*, 2015, **11**, 237-243.
53. N. S. K. Gowthaman and S. A. John, *RSC Adv.*, 2015, **5**, 42369-42375.
54. Y. Ding, Y. Wang, L. Zhang, H. Zhang, C. M. Li and Y. Lei, *Nanoscale*, 2011, **3**, 1149-1157.
55. A. Navaee, A. Salimi, S. Soltanian and P. Servati, *J Power Sources*, 2015, **277**, 268-276.
56. L. Yan, X. Bo, D. Zhu and L. Guo, *Talanta*, 2014, **120**, 304-311.
57. Y. Chen, J. Xu, X. Liu, Y. Tang and T. Lu, *Appl. Catal. B-Environ.*, 2013, **140–141**, 552-558.
58. M. Zheng, P. Li, G. Fu, Y. Chen, Y. Zhou, Y. Tang and T. Lu, *Appl. Catal. B-Environ.*, 2013, **129**, 394-402.
59. J. Xu, X. Wu, G. Fu, X. Liu, Y. Chen, Y. Zhou, Y. Tang and T. Lu, *Electrochim. Acta*, 2012, **80**, 233-239.
60. F. Zhang, Y. Zhou, Y. Chen, Z. Shi, Y. Tang and T. Lu, *J. Colloid Interf. Sci.*, 2010, **351**, 421-426.
61. L. Zhou, X. Lin, T. Huang and A. Yu, *J. Mater. Chem. A*, 2014, **2**, 5117-5123.
62. M. Zheng, Y. Chen, Y. Zhou, Y. Tang and T. Lu, *Talanta*, 2010, **81**, 1076-1080.

Graphic abstract

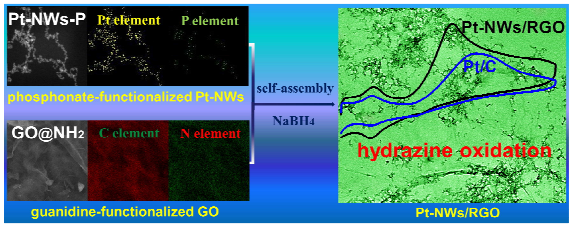

Pt-NWs-P can self-assemble on GO@NH_2 surface. After $NaBH_4$ reduction, Pt-NWs/RGO show improved electrocatalytic activity for the hydrazine oxidation reaction.